JMEPEG
https://doi.org/10.1007/s11665-024-09530-3

1059-9495/$19.00

ORIGINAL RESEARCH ARTICLE

# Prediction of Phase Formation Sequence in Multicomponent NiCoW/$Nb_3Al$ Interface

*Xiao Liu, Boning Zhang, Guowei Wang, Lan Liu, Yan Tang, and Lei Zheng*

Submitted: 1 December 2023 / Revised: 27 February 2024 / Accepted: 28 March 2024

**The interdiffusion behavior between NiCoW alloy and $Nb_3Al$ at 1000 °C was investigated. Based on the effective heat of formation model, the compounds at the interface are analyzed by calculating the effective heat of formation and establishing the map of favorable compound formation. It is concluded that the formation sequence of phases between the nickel-based alloy and $Nb_3Al$ is $Ni_6Nb_7$ → $Co_2Nb/Ni_6Nb_7$ + $Nb_{ss}$ → $Ni_3Nb$ → W-rich phase. The results of this paper provide a reference for the phase formation sequence law of multicomponent interface between $Nb_3Al$ and the matrix alloy.**

**Keywords** effective heat of formation, interdiffusion, interface, phase formation sequence

## 1. Introduction

$Nb_3Al$ has been widely studied as an ultra-high-temperature structural material (Ref 1-4). Besides high strength and creep resistance (Ref 2), $Nb_3Al$ was shown to be characterized by high melting point (2233 K) (Ref 1), low density (7.29 g/cm$^3$) (Ref 3), and high hardness (910 HV) (Ref 5). These properties of $Nb_3Al$ exhibit obvious advantages compared with the strengthening phase γ′-$Ni_3Al$ widely used in the nickel-based superalloys. Therefore, $Nb_3Al$ exhibits the potential to be used as a strengthening phase to replace the γ′-$Ni_3Al$ phase to obtain a new kind of nickel-based superalloy with stronger temperature-bearing capacity. The most important challenge of using δ-$Nb_3Al$ as a strengthening phase of nickel-based superalloy is to maintain the stability of δ-$Nb_3Al$ in the alloy. Different from the coarsening and instability of γ′-$Ni_3Al$ during long-term aging, δ-$Nb_3Al$ in the nickel-base superalloy may react with the matrix alloy to form new intermetallic compounds during the preparation and service process. At present, there are many reports about the interface reaction between intermetallic compounds, alloys, and metals (Ref 6-10). For example, McGregor et al. (Ref 6) found that the diffusion zone containing β-NiAl and $Ni_2TaAl$ was formed between CMSX-4 and NiTaAl. Ren et al. (Ref 7) reported that diffusion bonding was achieved between $Ti_2AlNb$ and nickel-based superalloy, while the thickness of diffusion zone was reduced by using Cu/Ti nano-laminated foil as the intermediate layer. Assari et al. (Ref 8) investigated the diffusion behavior at the interface between Ti and Al layers and found that the growth kinetics of the $TiAl_3$ diffusion layer formed at the interface accords with parabolic law. It is well known that the interface structure is directly related to the mechanical properties of materials (Ref 11, 12). Therefore, it is necessary to investigate the diffusion interface structure between the δ-$Nb_3Al$ and matrix alloy.

A variety of intermetallic compounds may be formed between different elements at the interface (Ref 13-17). Meanwhile, the type and formation order of the intermetallic compounds determine the interface structure (Ref 16, 18-21). Pretorius et al. (Ref 13, 14) first put forward an EFH model to predict the formation sequences of intermetallic compounds in the binary system. Bhanumurthy et al. (Ref 17) modified the EFH model by introducing the congruent factor, which improved the prediction accuracy of the model. Mogilevsky et al. (Ref 22) extended the effective formation heat model to ternary system. The semiquantitative analysis results of the model are in good correlation with the experimental results observed in systems such as Ta-SiC. However, the current analysis for the formation order of intermetallic compounds at multicomponent interfaces is limited to qualitative analysis (Ref 23, 24).

In this paper, the interdiffusion behavior between NiCoW alloy and $Nb_3Al$ was investigated. The phase formation sequence of the multielement NiCoW alloy/$Nb_3Al$ interface was analyzed based on the alloy composition and the Mogilevsky model. The results of this paper provide a reference for the phase formation sequence law of multielement interface between $Nb_3Al$ and the matrix alloy and contribute to evaluation the properties of novel nickel-based superalloy with δ-$Nb_3Al$ as strengthening phase.

## 2. Experiment

Interdiffusion experiments of $Nb_3Al$ block and nickel-based alloy block were carried out to simulate the interdiffusion behavior between δ-$Nb_3Al$ strengthening phase and matrix alloy in the novel δ-$Nb_3Al$ phase-strengthened nickel-based superalloy. The nickel-based alloy used in this study is Ni-25.3Co-15.8W (at.%) alloy prepared by electric arc furnace melting. Cylindrical samples with a diameter of 10 mm and a height of 10 mm were cut from the ingot by wire electrical

**Xiao Liu, Boning Zhang, Guowei Wang, Lan Liu, Yan Tang,** and **Lei Zheng**, School of Materials Science and Engineering, University of Science and Technology Beijing, Beijing 100083, China. Contact e-mails: zhangboning142703@163.com and zhenglei_ustb@sina.com.



Published online: 09 May 2024

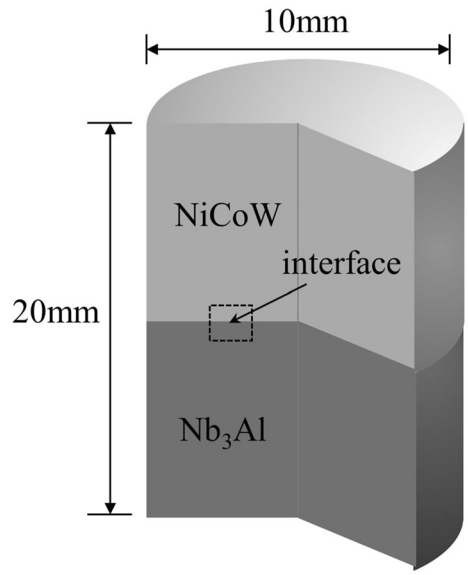


**Fig. 1** Assembly schematic diagram of the interdiffusion specimen

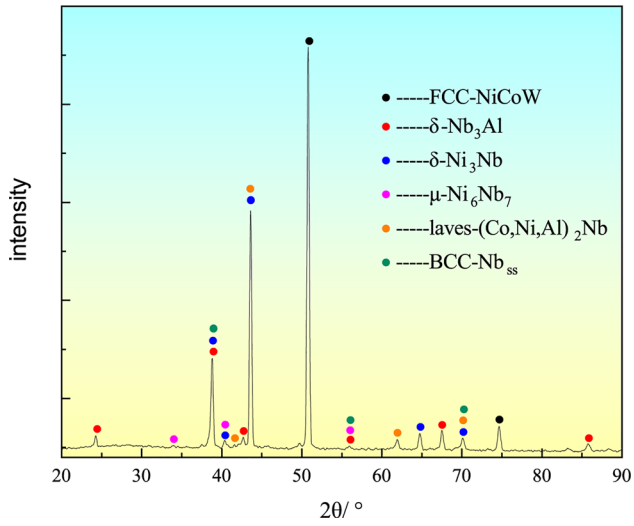


**Fig. 2** XRD pattern of the NiCoW/$Nb_3Al$ interface

discharge machining (WEDM). Cylindrical $Nb_3Al$ blocks of the same size were prepared by spark plasma sintering (SPS) with $Nb_3Al$ powder as raw material. The parameters of SPS were 1200 °C, 30 MPa and 5 min. Before the interdiffusion experiment, the nickel-based alloy and $Nb_3Al$ bulk samples were both ground with 400-2000# SiC sandpaper and then ultrasonic cleaned with ethanol. The interdiffusion experiment was carried out in Gleeble-3500 thermal simulation machine. The experimental parameters were 1000 °C, 30 MPa, 1 h. After the interdiffusion, all samples were cooled to room temperature in the Gleeble-3500 thermal simulation machine. The assembly schematic diagram of the interdiffusion specimen is shown in Fig. 1. The metallographic sample was cut from the diffusion interface marked in Fig. 1 by WEDM, grounded and polished. X-ray diffraction (XRD) was used to identify the microstructure of diffusion interface. The microstructure of the samples was characterized by scanning electron microscope (SEM) and energy-dispersive spectrometer (EDS).

## 3. Results

Figure 2 displays the XRD pattern of the NiCoW/$Nb_3Al$ interface. The $Ni_3Nb$, $Ni_6Nb_7$, and $Co_2Nb$ are identified along with the FCC structure of NiCoW alloy and the δ-$Nb_3Al$. The morphology of diffusion zone formed between NiCoW and $Nb_3Al$ is shown in Fig. 3. Five diffusion layers are visible according to the contrast difference, as named as I-V (shown in Fig. 3a). It can be seen that bright phases with granular and rod shape are distributed in the diffusion layer I. Meanwhile, according to the contrast, the diffusion layers II-IV are composed of single phase, while the diffusion layer V is composed of two phases. The total thickness of the diffusion zone is 23.45 $\mu$m. The thickness of the diffusion layer I-V is 8.56 $\mu$m, 4.71 $\mu$m, 3.85 $\mu$m, 2.39 $\mu$m, and 3.94 $\mu$m, respectively. Figure 3(b) shows the result of the line scan of the elemental distribution of the NiCoW/$Nb_3Al$ interface. It is found that the element distribution in diffusion layer I close to NiCoW alloy is the same as that in NiCoW alloy, while that in the region close to diffusion layer II is consistent with that in diffusion layer II. The elements in diffusion layer II are evenly distributed, and there is no noticeable fluctuation. This indicates that the phase composition range in diffusion layer II is narrow. However, the distribution of elements in diffusion layer III fluctuates obviously. This indicates that the phase composition range in diffusion layer III is wide. Figure 3(c) shows the elements distribution map of the NiCoW/$Nb_3Al$ interface. The results reveal that the contents of Ni, Co, and W gradually decrease and the content of Nb gradually increases along the direction from the NiCoW alloy to the $Nb_3Al$. Overall, the regions close to the NiCoW alloy show relatively low concentrations of Al, and it is noted that the diffusion zone I exhibits a slightly higher Al content than adjacent regions. The diffusion layer I is obviously rich in W, while Ni, Co, Nb, and Al are less. There is an obvious W-rich region in diffusion layer I, where Ni, Co, Nb, and Al are less.

Figure 4 displays the high magnification images of diffusion layer I and diffusion layer V, respectively. Figure 4(a) confirms that there are two phases in the diffusion layer I besides the granular-like and rod-like bright phase. Figure 4(b) displays that the light phase and dark phase in the diffusion layer V are distributed alternately. It can be seen that the elements contents, especially the content of Nb, are quite different between the two phases in the diffusion layer V. Combined with the EDS results and phase composition in the phase diagram, it is shown from Fig. 3(a) that the bright phase in diffusion zone I is W-rich phase and the dark phase is $Ni_3Nb$. The EDS results of positions marked in Fig. 3 and 4 are listed in Table 1. Combining the EDS and XRD results, the bright phase in diffusion zone I is identified as W-rich phase. The gray phase is FCC-structured phase of the NiCoW alloy and the dark phase adjacent to the diffusion layer II is identified as $Ni_3Nb$. Meanwhile, the phase in diffusion layer II is identified as $Ni_3Nb$, the phase in diffusion layer III is identified as $Co_2Nb$, and the phase in diffusion layer IV is identified as $Ni_6Nb_7$. The phases in diffusion layer V are $Ni_6Nb_7$ (dark phase) and $Nb_{ss}$ (bright phase, the BCC phase of Nb with slight solid solutions of Ni and Co). The formation process of each phase at the interface is analyzed in the discussion section. To summarize, the diffusion interface structure between the nickel-based alloy

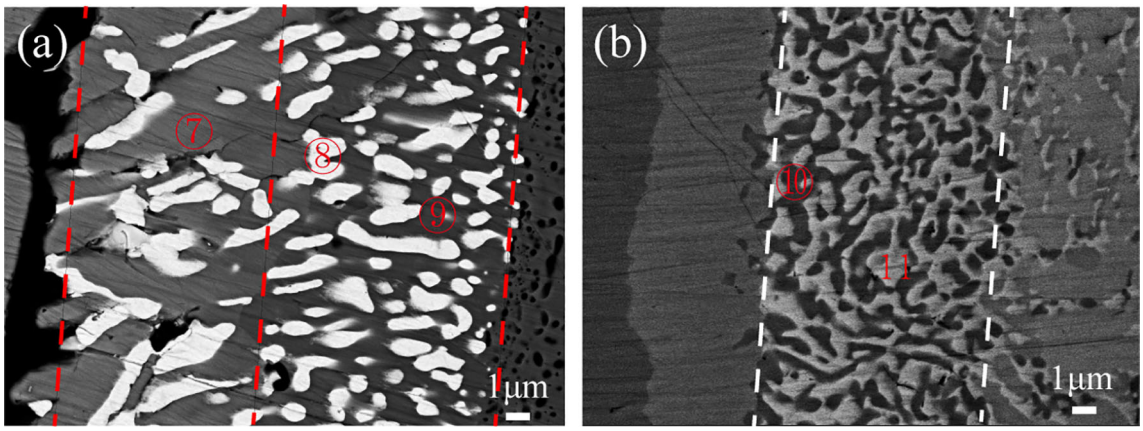


**Fig. 3** Microstructure and elements distribution of interface region between the NiCoW alloy and $Nb_3Al$. (①-⑥ indicate the EDS detection position, and I-V indicate different areas at the interface) (a) Microstructure of NiCoW/$Nb_3Al$ interface; (b) Line-scan result of NiCoW/$Nb_3Al$ interface; and (c) Elements distribution of NiCoW/$Nb_3Al$ interface

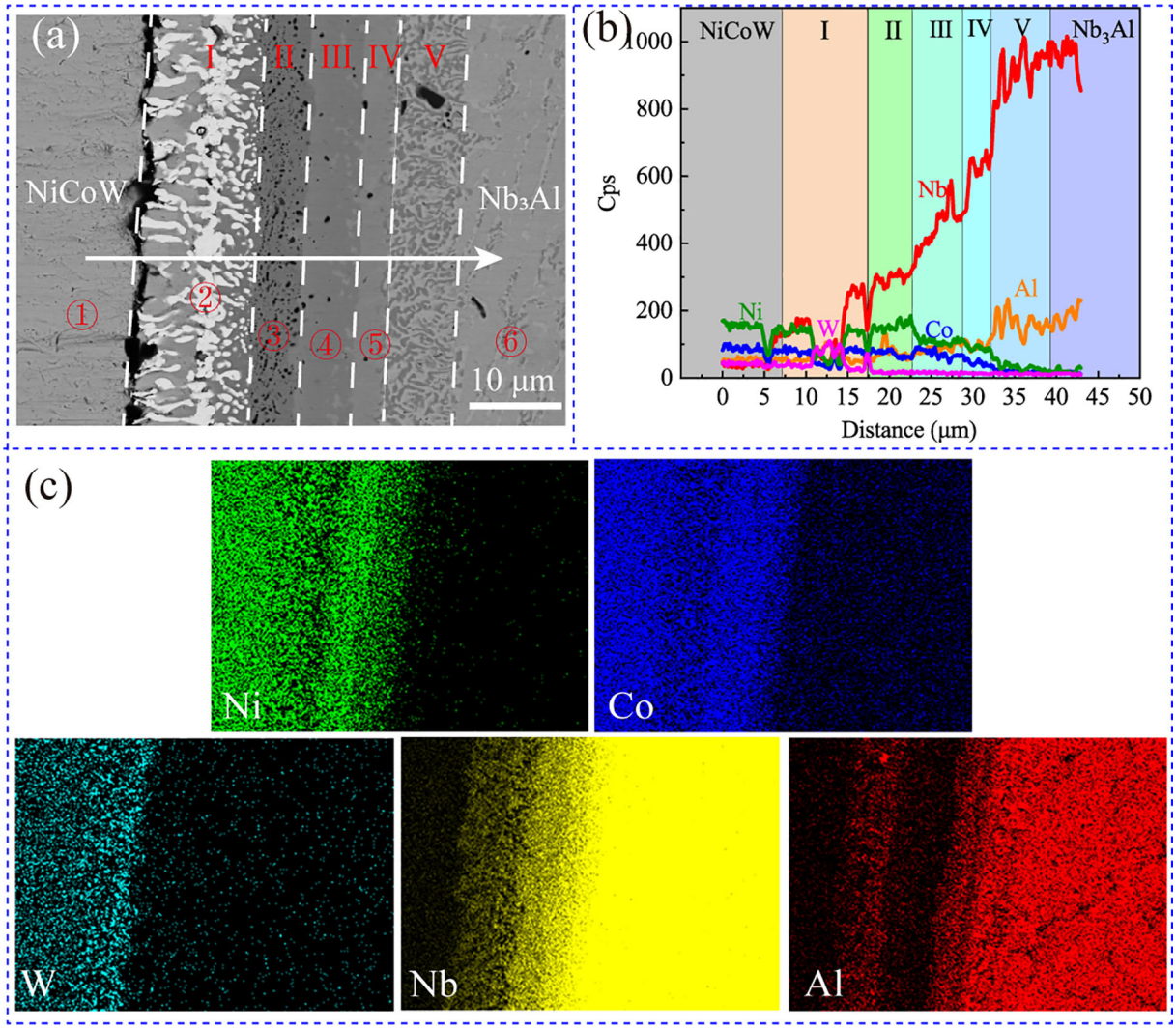


**Fig. 4** High magnification images of (a) diffusion layer I and (b) diffusion layer V

**Table 1 EDS results (at.%) of the marked locations in Fig. 3 and 4**

| | Ni | Co | W | Nb | Al |
|---|---|---|---|---|---|
| 1 | 58.38 | 24.26 | 17.36 | 0.00 | 0.00 |
| 2 | 11.60 | 4.20 | 84.20 | 0.00 | 0.00 |
| 3 | 51.06 | 21.67 | 0.87 | 24.39 | 2.01 |
| 4 | 36.10 | 19.22 | 0.65 | 34.43 | 9.61 |
| 5 | 29.37 | 10.65 | 0.00 | 49.31 | 10.67 |
| 6 | 0.00 | 0.00 | 0.00 | 80.27 | 19.73 |
| 7 | 58.38 | 25.26 | 17.36 | 0.00 | 0.00 |
| 8 | 11.60 | 4.20 | 84.20 | 0.00 | 0.00 |
| 9 | 52.55 | 22.88 | 0.82 | 22.45 | 1.32 |
| 10 | 30.35 | 12.34 | 2.89 | 46.87 | 7.55 |
| 11 | 7.06 | 1.46 | 0.00 | 86.56 | 4.92 |

and $Nb_3Al$ is composed of NiCoW/W-rich phase/$Ni_3Nb$/$Co_2Nb$/$Ni_6Nb_7$/$Ni_6Nb_7$ + $Nb_{ss}$/$Nb_3Al$.

## 4. Discussion

At the initial stage of diffusion between the NiCoW alloy and the $Nb_3Al$ intermetallic compound, atoms from the two materials form a mixed interface and new compounds under the driving force of chemical potential gradient (Ref 23). According to phase diagrams (Ref 24), Ni, Co, and W atoms in NiCoW are anticipated to react with Nb and Al atoms in $Nb_3Al$ to form various compounds at 1000 °C. The formation order of compounds determines the interface structure (Ref 25). Here, the formation order of different compounds can be evaluated by the effective heat of formation $\Delta H\prime$ (Ref 26), which is defined as:

$$\Delta H\prime = \left(\Delta H^0 + \Delta H^f\right) C_e / C_1 \quad \text{(Eq 1)}$$

where $\Delta H^0$ is the standard heat of formation, $C_e$ is the effective concentration of the controlling element at the interface, $C_1$ is the limiting element concentration in the compound, and $\Delta H^f$ represents the congruency factor, which is zero for non-congruent compounds but proportional to the melting point $T_m$ of congruent compounds as (Ref 16):

$$\Delta H^f = 8.13 T_m \quad \text{(Eq 2)}$$

The effective concentration $C_e$ is mainly influenced by element content and diffusion coefficient (Ref 21). Then, the effective concentration at the interface can be compared according to these two parameters. Because the diffusion coefficient of W in the nickel-based alloy is two orders of magnitude lower than that of Ni and Co (Ref 26), the relatively low content of W in the mixed reaction layer at the interface can be ignored. Meanwhile, the diffusion coefficients of Ni and Co in Ni-based alloy are close, but the Ni concentration is obviously higher than that of Co. Therefore, the mixed reaction layer formed at the initial stage of reaction between NiCoW and $Nb_3Al$ is approximated as a Ni-$Nb_3Al$ system. For such a ternary system, the formation sequence of phases at the interface can be analyzed according to the model proposed by Mogilevsky (Ref 21).This is determined by the effective heat of formation obtained on the vertical section of the Ni-$Nb_3Al$ and the $X_{Nb}/X_{Al}$ for the most favorable compound formation map (Ref 21). $X_{Nb}$ and $X_{Al}$ refer to the effective concentrations of Nb and Al, respectively. $X_{Nb}/X_{Al}$ is used to determine the compound region in the most favorable compound formation map. The effective heat of formation of the compounds obtained on the vertical section of the Ni-$Nb_3Al$ is listed in Table 2, and the values of $X_{Nb}/X_{Al}$ are listed in Table 3. The map of favorable compound formation and the effective heat of formation diagram for Ni-$Nb_3Al$ are depicted in Fig. 5. It is noteworthy that the effective heats of formation for $Ni_2Al_3$, NiAl, and $Ni_3Al$ in the Ni-Al system surpass those of $Ni_6Nb_7$ and $Ni_3Nb$ in the Ni-Nb system. Following the criteria of the model, since the favorable formation regions of compounds in the Ni-Al system are situated farther from the Ni-$Nb_3Al$ line compared to those in the Ni-Nb system (as illustrated in Fig. 4a), compounds in the Ni-Nb system are formed prior to those in the Ni-Al system (Ref 21). Furthermore, the effective heat of formation of $Ni_3Nb$ is smaller than that of $Ni_6Nb_7$, as indicated in Fig. 7(b). Hence, $Ni_6Nb_7$ is initially formed at the initial interface of NiCoW/$Nb_3Al$, leading to the appearance of the interface structure of NiCoW/$Ni_6Nb_7$/$Nb_3Al$.

**Table 2 Free energy of formation, $\Delta H^0$, and the effective free heat of formation on the vertical section of the Ni-$Nb_3Al$ system, $\Delta H\prime$**

| Phase | $\Delta H^0$, kJ/(mol. at.) | $\Delta H\prime$, kJ/(mol. at.) |
|---|---|---|
| $Ni_6Nb_7$ | − 20.76 (Ref 27) | − 15.47 |
| $Ni_3Nb$ | − 16.42 (Ref 27) | − 15.15 |
| $Ni_2Al_3$ | − 57.00 (Ref 27) | − 20.35 |
| NiAl | − 43.33 (Ref 27) | − 17.33 |
| $Ni_3Al$ | − 27.63 (Ref 27) | − 15.78 |

**Table 3 Data necessary for constructing projections of effective free energy of formation diagrams**

| Compounds | $X_{Nb}/X_{Al}$ |
|---|---|
| $Ni_3Nb$-$Ni_3Al$ | 1.34 |
| $Ni_3Nb$-NiAl | 0.96 |
| $Ni_3Nb$-$Ni_2Al_3$ | 0.77 |
| $Ni_6Nb_7$-$Ni_3Al$ | 4.25 |
| $Ni_6Nb_7$-NiAl | 3.06 |
| $Ni_6Nb_7$-$Ni_2Al_3$ | 2.46 |

After the formation of the interface structure of NiCoW/$Ni_6Nb_7$/$Nb_3Al$, the phases at the new interfaces of $Ni_6Nb_7$/$Nb_3Al$ and NiCoW/$Ni_6Nb_7$ were analyzed, respectively. Since the diffusion rates of Ni and Co in $Ni_6Nb_7$ (Ref 27) are similar but the content of Ni in NiCoW alloy is much higher than that of Co, the content of Ni diffused from NiCoW to the $Ni_6Nb_7$/$Nb_3Al$ interface is higher than that of Co. Therefore, the content of Ni is higher than that of Co at the interface of $Ni_6Nb_7$/$Nb_3Al$. The mixed reaction layer at the interface of $Ni_6Nb_7$/$Nb_3Al$ can be considered as Ni-$Nb_3Al$ system. Considering that Ni and Co in the NiCoW diffuse through $Ni_6Nb_7$ to the interface of $Ni_6Nb_7$/$Nb_3Al$, the contents of Ni and Co at the interface are lower than those at the initial interface of NiCoW/$Nb_3Al$.

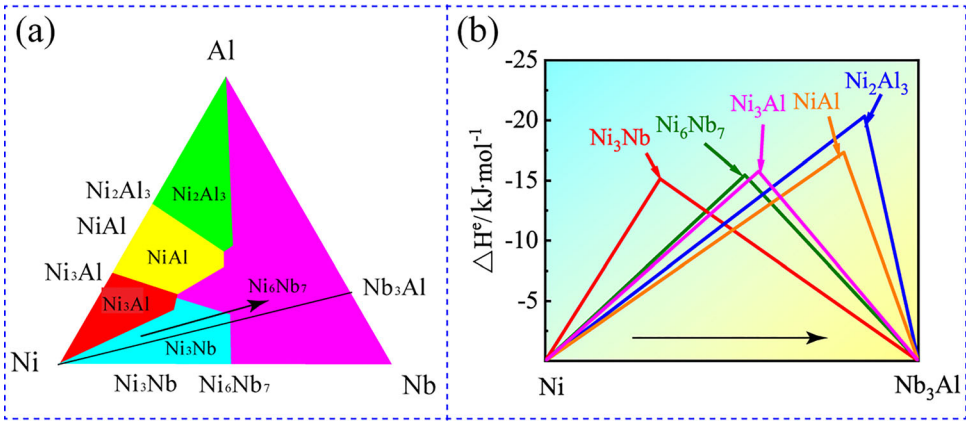


**Fig. 5** Analysis basis for compound formation sequence in Ni-$Nb_3Al$ system. (a) Map of favorable compound formation; (b) Vertical section of the effective heat of formation diagram

**Table 4 Free energy of formation, $\Delta H^0$ (Ref 27), and the effective free heat of formation on the vertical section of the Co-$Ni_6Nb_7$ system, $\Delta H'$**

| Phase | $\Delta H^0$, KJ/(mol. at.) | $\Delta H'$, KJ/(mol. at.) |
|---|---|---|
| $Co_7Nb_6$ | − 23.20 | − 16.62 |
| $Co_2Nb$ | − 42.72 | − 33.19 |
| $Co_3Nb$ | − 45.00 | − 28.06 |

Therefore, the composition at the interface of $Ni_6Nb_7/Nb_3Al$ proceeds in the direction favorable to the formation of $Ni_6Nb_7$ (the direction marked by arrows in Fig. 5) and $Ni_6Nb_7$ continues to be generated at the interface of $Ni_6Nb_7/Nb_3Al$. Given that Nb consumption through formation of $Ni_6Nb_7$ phase and diffusion to NiCoW alloy is slower than Nb generation from $Nb_3Al$ decomposition, Nb undergoes local enrichment at the $Ni_6Nb_7/Nb_3Al$ interface. These Nb atoms then precipitate as a solid solution ($Nb_{ss}$) and intermix with $Ni_6Nb_7$, resulting in the formation of the two-phase structure in layer V. At the NiCoW/$Ni_6Nb_7$ interface, the mixed reaction layer can be considered as Co-$Ni_6Nb_7$ ternary system. Therefore, the formation sequence of phase can be analyzed according to the model proposed by Mogilevsky (Ref 21). In addition, the reaction in Eq 1 also occurs at the interface according to the phase diagram of Ni-Nb (Ref 28).

$$Ni + Ni_6Nb_7 \rightarrow Ni_3Nb \qquad \text{(Eq 3)}$$

The heat of formation in Eq 3 is − 8.73 kJ/(mol. at.) (Ref 28). Due to the formation of ideal solid solution between Ni and Co (Ref 26), no compounds are formed between them, the map of favorable formation of compounds at the Co-$Ni_6Nb_7$ interface cannot be distinguished. Meanwhile, the effective heat of formation of compounds on the section of Co-$Ni_6Nb_7$ is calculated and shown in Table 4 and Fig. 6. It is revealed that $Co_2Nb$ has the largest effective heat of formation in the compounds of Co-$Ni_6Nb_7$ ternary system, while the effective heat of formation of $Co_2Nb$ is also larger than that of $Ni_3Nb$. Therefore, $Co_2Nb$ is formed at the interface of NiCoW/$Ni_6Nb_7$ and the interface structure composed of NiCoW/$Co_2Nb$/$Ni_6Nb_7$/$Ni_6Nb_7$ + $Nb_{ss}/Nb_3Al$ forms.

The formation of the interface structure of NiCoW/$Co_2Nb$/$Ni_6Nb_7$/$Ni_6Nb_7$ + $Nb_{ss}/Nb_3Al$ gives rise to new interfaces,

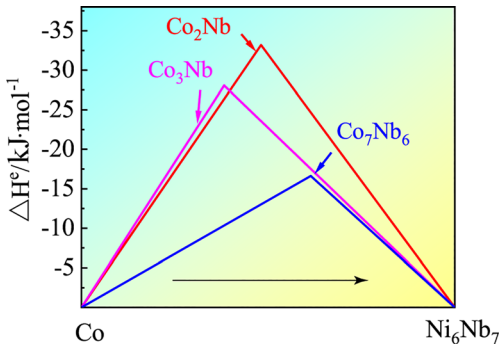


**Fig. 6** Vertical section of the effective heat of formation diagram for Co-$Ni_6Nb_7$ system

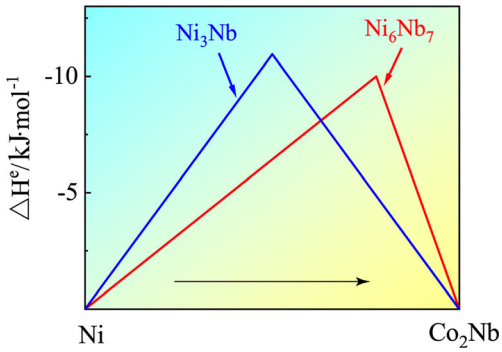


**Fig. 7** Vertical section of the effective heat of formation diagram for Ni-$Co_2Nb$ system

including $Ni_6Nb_7$ + $Nb_{ss}/Nb_3Al$, $Co_2Nb/Ni_6Nb_7$, and NiCoW/$Co_2Nb$. In comparison with the $Ni_6Nb_7/Nb_3Al$ interface, there is a further reduction in the Ni and Co contents at the interface of $Ni_6Nb_7$ + $Nb_{ss}/Nb_3Al$. Consequently, the composition of the mixed reaction layer continues to proceed in favor of $Ni_6Nb_7$ formation, as indicated by the arrows in Fig. 7. Consequently, $Ni_6Nb_7$ and $Nb_{ss}$ continue to be generated at the interface. Additionally, since Ni and Co do not form compounds, the mixed reaction layer at the interface of $Co_2Nb/Ni_6Nb_7$ can still be considered as Co-$Ni_6Nb_7$ ternary system. Unlike the NiCoW/$Ni_6Nb_7$ interface, the Ni and Co contents at the $Co_2Nb/Ni_6Nb_7$ interface are reduced. Hence, the composition

proceeds in favor of $Co_2Nb$ formation, as indicated by the arrows in Fig. 6, and $Co_2Nb$ continues to form at the interface of $Co_2Nb/Ni_6Nb_7$. Moreover, the NiCoW/$Co_2Nb$ interface can be viewed as a Ni-$Co_2Nb$ ternary system, and the phase formation sequence is analyzed according to the model proposed by Mogilevsky (Ref 21). The reaction in Eq 2 also occurs at the interface according to the phase diagram of Co-Nb (Ref 25).

$$Co + Co_2Nb \rightarrow Co_3Nb \quad \text{(Eq 4)}$$

The heat of formation in Eq 4 is − 7.87 kJ/(mol. at.) (Ref 25). Figure 7 and Table 5 present the map of favorite compound formation and the vertical section of the effective heat of formation diagram for Ni-$Co_2Nb$, respectively. Similar to the Co-$Ni_6Nb_7$ system, the lack of Ni-Co compounds prevents the acquisition of a favorite formation diagram for the Ni-$Co_2Nb$ system. The effective heat of formation of each compound on the Ni-$Co_2Nb$ section is displayed in Table 5 and Fig. 7. Notably, $Ni_3Nb$ exhibits the highest effective heat of formation among the compounds in the Ni-$Co_2Nb$ ternary system, surpassing that of the reaction between Co and $Co_2Nb$ to produce $Co_3Nb$. Consequently, $Ni_3Nb$ is formed at the NiCoW/$Co_2Nb$ interface, resulting in the interface structure of NiCoW/$Ni_3Nb/Co_2Nb/Ni_6Nb_7/Ni_6Nb_7 + Nb_{ss}/Nb_3Al$ (Table 6).

With the formation of the interface structure of NiCoW/$Ni_3Nb/Co_2Nb/Ni_6Nb_7/Ni_6Nb_7 + Nb_{ss}/Nb_3Al$, new interfaces of $Ni_3Nb/Co_2Nb$ and NiCoW/$Ni_3Nb$ emerge. Due to the reduction of the content of Ni and Co at the $Ni_3Nb/Co_2Nb$ interface compared with that of the NiCoW/$Co_2Nb$ interface, the composition of the mixed reaction layer continues to proceed in the direction favorable to the formation of $Ni_3Nb$ (as indicated by the arrows in Fig. 7). Consequently, $Ni_3Nb$ continue to be generated at the interface. Meanwhile, the mixed reaction layer at the interface of NiCoW/$Ni_3Nb$ can be considered as Nb-$Ni_{2.32}Co$ ternary system, and the phase formation sequence is analyzed following the model proposed by Mogilevsky (Ref 21). The map of favorite compound formation and vertical section of the effective heat of formation diagram for Nb-$Ni_{2.32}Co$, along with the necessary data for drawing, are presented in Fig. 8, Tables 6 and 7, respectively. It is evident that $Ni_3Nb$ exhibits the highest effective heat of formation along the compounds in the Nb-$Ni_{2.32}Co$ ternary system, confirming its formation at the interface of Nb-$Ni_{2.32}Co$. Additionally, as Ni and Co diffuse within the NiCoW alloy toward the $Nb_3Al$, W precipitates in the NiCoW alloy close to the interface of NiCoW/$Ni_3Nb$, resulting in the formation of a W-rich phase. In summary, the interface structure of NiCoW/W-rich phase/$Ni_3Nb/Co_2Nb/Ni_6Nb_7/Ni_6Nb_7 + Nb_{ss}/Nb_3Al$ is established. Figure 9 illustrates the schematic diagram of the formation sequence of compounds at the NiCoW/$Nb_3Al$ interface, where the sequence proceeds as follows: $Ni_6Nb_7 \rightarrow Co_2Nb/Ni_6Nb_7 + Nb_{ss} \rightarrow Ni_3Nb \rightarrow$ W-rich phase (Table 7).

**Table 5 Free energy of formation, $\Delta H^0$ (Ref 27), and the effective free heat of formation on the vertical section of the Ni-$Co_2Nb$ system, $\Delta H'$**

| Phase | $\Delta H^0$, kJ/(mol. at.) | $\Delta H'$, kJ/(mol. at.) |
|---|---|---|
| $Ni_6Nb_7$ | − 20.76 | − 10.00 |
| $Ni_3Nb$ | − 16.42 | − 10.95 |

**Table 6 Free energy of formation, $\Delta H^0$ (Ref 27), and the effective free heat of formation on the vertical section of the Nb-$Ni_{2.32}Co$ system, $\Delta H'$**

| Phase | $\Delta H^0$, kJ/(mol. at.) | $\Delta H'$, kJ/(mol. at.) |
|---|---|---|
| $Ni_6Nb_7$ | − 20.76 | − 13.83 |
| $Ni_3Nb$ | − 16.42 | − 14.38 |
| $Co_7Nb_6$ | − 23.20 | − 9.67 |
| $Co_2Nb$ | − 42.72 | − 16.89 |
| $Co_3Nb$ | − 45.00 | − 16.53 |

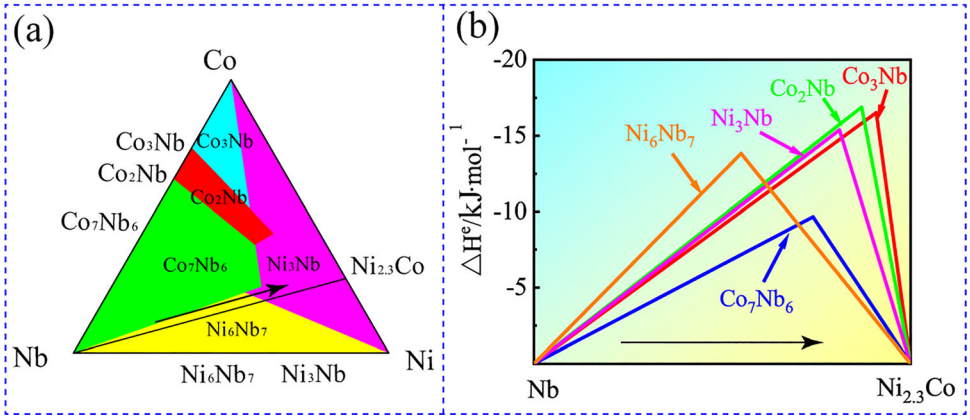


**Fig. 8** Analysis basis for compound formation sequence in Nb-$Ni_{2.32}Co$ system. (a) Map of favorable compound formation; (b) Vertical section of the effective heat of formation diagram for Nb-$Ni_{2.32}Co$ system

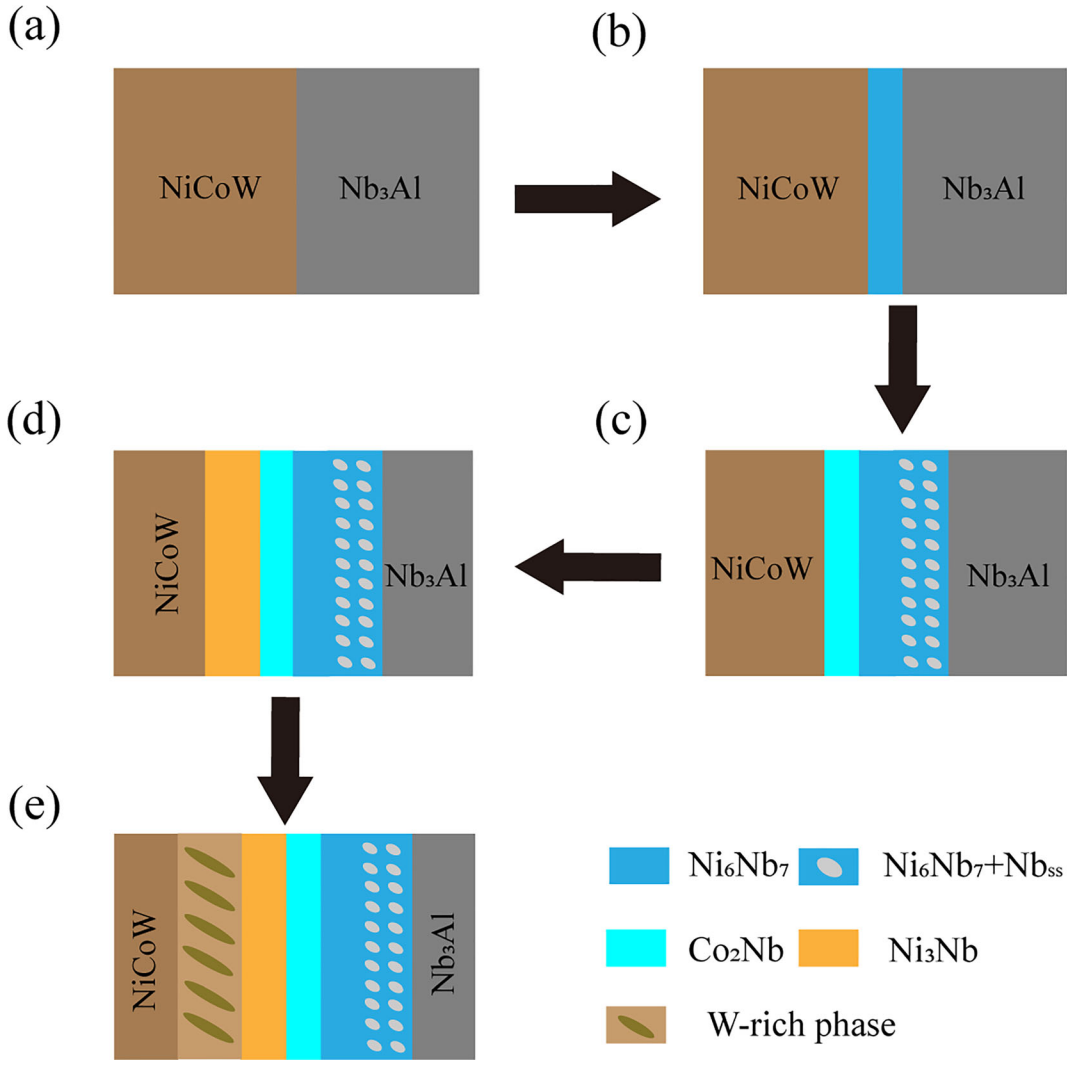


**Fig. 9** Schematic diagram of the formation sequence of compounds at the NiCoW/$Nb_3Al$ interface

**Table 7 Data necessary for constructing projections of effective free energy of formation diagrams for Nb-$Ni_{2.3}Co$ system**

| Compounds | $X_{Ni}/X_{Co}$ |
|---|---|
| $Ni_3Nb$-$Co_7Nb_6$ | 1.968 |
| $Ni_3Nb$-$Co_2Nb$ | 2.927 |
| $Ni_3Nb$-$Co_3Nb$ | 2.741 |
| $Ni_6Nb_7$-$Co_7Nb_6$ | 0.958 |
| $Ni_6Nb_7$-$Co_2Nb$ | 1.425 |
| $Ni_6Nb_7$-$Co_3Nb$ | 1.334 |

## 5. Conclusions

The diffusion interface of NiCoW/W-rich phase/$Ni_3Nb$/$Co_2Nb$/$Ni_6Nb_7$/$Ni_6Nb_7$ + $Nb_{ss}$/$Nb_3Al$ was formed between the NiCoW alloy and $Nb_3Al$ at 1000 °C for 1 h.

Based on the effective heat of formation (EHF) model, the compounds at the interface are analyzed by calculating the effective heat of formation and establishing the map of favorable compound formation. The formation sequence of compounds at the NiCoW/$Nb_3Al$ interface is confirmed to be $Ni_6Nb_7$ → $Co_2Nb$/$Ni_6Nb_7$ + $Nb_{ss}$ → $Ni_3Nb$ → W-rich phase.


### Acknowledgments

The authors gratefully appreciate the financial supports by National Natural Science Foundation of China (No. 52171094, No. 52301176), Fundamental Research Funds for the Central Universities (No. FRF-TP-22-006C2), and National Natural Science Foundation of China (No. U23A6016).


### Author Contributions

Xiao Liu contributed to conceptualization, methodology, data curation, formal analysis, and writing—original draft. Boning Zhang was involved in resources, writing—review and editing, project administration, funding acquisition, and supervision. Guowei Wang contributed to supervision and writing—review

and editing. Lan Liu was involved in conceptualization, supervision, and writing—review & editing. Yan Tang contributed to supervision and writing—review and editing. Lei Zheng was involved in project administration, resources, writing—review and editing, project administration, funding acquisition, and supervision.

## Data Availability

The authors do not have permission to share data.

## Conflict of interest

The authors declare that they have no known competing financial interests or personal relationships that could have appeared to influence the work reported in this paper.

## References


1. D.L. Anton, A.F. Giamel, D.M. Shah, and D.N. Duhl, Selecting High-Temperature Structural Intermetallic Compounds: The Engineering Approach, *JOM*, 1989, **41**, p 12–17.
2. D. Shah and D. Anton, Evaluation of Refractory Intermetallics with A15 Structure for High Temperature Structural Applications, *Mat. Sci. Eng. A-Struct.*, 1992, **153**, p 402–409.
3. D.P. Pope and R. Darolia, High-Temperature Applications of Intermetallic Compounds, *MRS Bull.*, 1996, **21**, p 30–36.
4. H. Bei, G.M. Pharr, and E.P. George, A Review of Directionally Solidified Intermetallic Composites for High-Temperature Structural Applications, *J. Mater. Sci.*, 2004, **39**, p 3975–3984.
5. D.M. Dimiduk, D.B. Miracle, and C.H. Ward, Development of Intermetallic Materials for Aerospace Systems, *Mater. Sci. Tech.*, 1992, **8**, p 367–375.
6. M.R. McGregor, M.E. Hancock, L. Pallett, and W.J. Clegg, Examination of Ni-Based Superalloy/Intermetallic Diffusion Couples Containing Multiphase Regions, *Intermetallics*, 2019, **113**, 106559
7. H.S. Ren, X.Y. Ren, H.P. Xiong, W.W. Li, S.J. Pang, and A.I. Ustinov, Nano-diffusion Bonding of $Ti_2AlNb$ to Ni-Based Superalloy, *Mater Charact*, 2019, **155**, 109813
8. A.H. Assari and B. Eghbali, Solid State Diffusion Bonding Characteristics at the Interfaces of Ti and Al Layers, *J. Alloy. Compd.*, 2019, **773**, p 50–58.
9. L. Xu, Y.Y. Cui, Y.L. Hao, and R. Yang, Growth of Intermetallic Layer in Multi-laminated Ti/Al Diffusion Couples, *Mat. Sci. Eng. A-Struct.*, 2006, **435**, p 638–647.
10. N. Thiyaneshwaran, K. Sivaprasad, and B. Ravisankar, Characterization Based Analysis on $TiAl_3$ Intermetallic Phase Layer Growth Phenomenon and Kinetics in Diffusion Bonded Ti/$TiAl_3$/Al Laminates, *Mater Charact*, 2021, **174**, 110981
11. W. Ding, N. Liu, J.C. Fan, J. Cao, and X.J. Wang, Diffusion Bonding of Copper to Titanium Using CoCrFeMnNi High-Entropy Alloy Interlayer, *Intermetallics*, 2021, **129**, 107027
12. Y.L. Zhang, X.S. Jiang, Y.J. Fang, H.L. Sun, T.F. Song, D.F. Mo, X. Li, and Z.P. Luo, Vacuum Diffusion Bonding of CoCrFeNiMo MEAs and Inconel718 Using Ni Interlayer, *Mater. Lett.*, 2020, **279**, 128509
13. R. Pretorius, C.C. Theron, and T.K. Marais, Evaluation of Anomalies during Nickel and Titanium Suicide Formation Using the Effective Heat of Formation Model, *Mater. Chem. Phys.*, 1993, **36**, p 31–38.
14. R. Pretorius, T.K. Marais, and C.C. Theron, Thin Film Compound Phase Formation Sequence: An Effective Heat of Formation Model, *Mat. Sci. Eng. R.*, 1993, **10**, p 1–83.
15. R. Pretorius, C.C. Theron, A. Vantomme, and J.W. Mayer, Compound Phase Formation in Thin Film Structures, *Crit. Rev. Solid State Mater. Sci.*, 1999, **24**, p 1–62.
16. K. Bhanumurthy, W. Krauss, and J. Konys, Solid-State Diffusion Reaction and Formation of Intermetallic Phases in the Fe-Al System, *Fusion Sci. Technol.*, 2014, **65**, p 262–272.
17. A. Laik, K. Bhanumurthy, and G.B. Kale, Intermetallics in the Zr–Al Diffusion Zone, *Intermetallics*, 2004, **12**, p 69–74.
18. R. Pretorius, R. De Reus, and A.M. Vredenberg, Use of the Effective Heat of Formation Rule for Predicting Phase Formation Sequence in Al-Ni Systems, *Mater. Lett.*, 1990, **9**, p 494–499.
19. R. Pretorius, A.M. Vredenberg, and F.W. Saris, Prediction of Phase Formation Sequence and Phase Stability In Binary Metal-Aluminum Thin-Film Systems Using the Effective Heat of Formation Rule, *J. Appl. Phys.*, 1991, **70**, p 3636–3646.
20. J.H. Zhu, C.T. Liu, L.M. Pike, and P.K. Liaw, Enthalpies of Formation of Binary Laves Phases, *Intermetallics*, 2002, **2002**, p 579–595.
21. P. Mogilevsky and E.Y. Gutmanas, First Phase Formation at Interfaces: Effective Heat of Formation Model for Ternary Systems, *Mat. Sci. Eng. A-Struct.*, 1996, **208**, p 203–209.
22. S.W. Park, Y.I. Kim, J.S. Kwak, and H.K. Baik, Investigation of Co/SiC Interface Reaction, *J. Electron. Mater.*, 1997, **26**, p 172–177.
23. P. Mogilevsky and E.Y. Gutmanas, On Thermodynamics of First-Phase Formation during Interfacial Reactions, *Mat. Sci. Eng. A-Struct.*, 1996, **221**, p 76–84.
24. X.S. Qi, X.Y. Xue, B. Tang, H.C. Kou, R. Hu, and J.S. Li, Phase Evolution of Diffusion Bonding Interface Between High Nb Containing TiAl Alloy and Ni-Cr-W Superalloy, *Rare. Metal. Mat. Eng.*, 2015, **44**, p 1575–1580.
25. R.K. Shaipov, E.Y. Kerimov, and E.M. Slyusarenko, Isothermal Sections of the Co-Nb-Ni Phase Diagram at 1200 and 1375 K, *J. Alloy. Compd.*, 2018, **742**, p 466–479.
26. W.Q. Li, S.P. Hu, Y.Z. Lei, L.E. Yu, X.G. Song, and J.C. Feng, Interfacial Microstructure and Mechanical Properties of GH99 Superalloy and Nb Brazed Joint Using Cu75Pt25 Filler, *T. Nonferr. Metal. Soc.*, 2020, **30**, p 2724–2736.
27. I. Barin, *Thermochemical Data of Pure Substances*, Springer, Weinheim, 1989
28. Y. Du, Y.A. Chang, W.P. Gong, B.Y. Huang, H.H. Xu, Z.P. Jin, and F. Zhang, Thermodynamic Properties of the Al-Nb-Ni System, *Intermetallics*, 2003, **11**, p 995–1013.